

Local Organization of Graphene Network Inside Graphene/Polymer Composites

Alexander Alekseev,* Delei Chen, Evgeniy E. Tkalya, Marcos G. Ghislandi, Yuliya Syurik, Oleg Ageev, Joachim Loos, and Gijbertus de With

The local electrical properties of a conductive graphene/polystyrene (PS) composite sample are studied by scanning probe microscopy (SPM) applying various methods for electrical properties investigation. We show that the conductive graphene network can be separated from electrically isolated graphene sheets (GS) by analyzing the same area with electrostatic force microscopy (EFM) and conductive atomic force microscopy (C-AFM). EFM is able to detect the graphene sheets below the sample surface with the maximal depth of graphene detection up to ≈ 100 nm for a tip-sample potential difference of 3 V. To evaluate depth sensing capability of EFM, the novel technique based on a combination of SPM and microtomy is utilized. Such a technique provides 3D data of the GS distribution in the polymer matrix with z-resolution on the order of ≈ 10 nm. Finally, we introduce a new method for data correction for more precise 3D reconstruction, which takes into account the height variations.

1. Introduction

The unique electrical, mechanical and other properties of graphene^[1–3] and its derivatives^[4,5] make it important to investigate the properties of polymer-based graphene composites. Different approaches for preparation and characterization of such composites have been proposed recently.^[6–12] Current state-of-the-art situation in the area of graphene-polymer composites has been described in several recent reviews.^[13–16] The methods

of preparation of a filler and matrix and the way of their mixing are of critical importance, since they determine the properties of the composite. Among others, electrical properties of composites attract great attention due to the large area of possible applications. Percolation behavior of conductivity in graphene/polymer composites has been revealed and analyzed by various research groups.^[6,8,10–12] Corresponding to the widely accepted percolation theory, charge transport inside the insulating polymer/conductive filler composites is executed through the conductive network formed by the filler.^[17,18] It means that the local organization of graphene sheets (GS) inside the polymer matrix is responsible for the conductive properties of the composite. Until now information about the distribution of graphene sheets

inside the polymer was obtained mostly by electron microscopy.^[6–12] Scanning probe microscopy methods were used in study of graphene/polymer composites only in few works.^[12] In the present study we use electrical methods of scanning probe microscopy (SPM) for analysis of the graphene network inside a conductive graphene/polystyrene (PS) composite. It is shown that the graphene sheets (GS), connected into the conductive network and isolated ones, can be distinguished by measurements of the same area with both conductive atomic

Dr. A. Alekseev
Laboratory of Materials and Interface Chemistry
Eindhoven University of Technology
Den Dolech 2, Eindhoven
5600 MB, The Netherlands
E-mail: alalrus@gmail.com

D. Chen, M. G. Ghislandi, Prof. G. de With
Laboratory of Materials and Interface Chemistry
Eindhoven University of Technology
Den Dolech 2, Eindhoven
5600 MB, The Netherlands

E. E. Tkalya
Department of Polymer Chemistry
Eindhoven University of Technology
Den Dolech 2, Eindhoven
5600 MB, The Netherlands

Y. Syurik, Prof. O. Ageev
Taganrog Institute of Technology
Shevchenko Street 2
Taganrog, 347928, Russia

Prof. J. Loos
School of Physics and Astronomy
Kelvin Nanocharacterisation Centre
and Scottish University Physics Alliance
University of Glasgow
University Avenue, Glasgow
G128QQ, UK



DOI: 10.1002/adfm.201101796

force microscopy (C-AFM) and electrostatic force microscopy (EFM). Peculiarities of EFM imaging on the graphene/polymer composites are analyzed and discussed. In our recent studies, only two-dimensional information was obtained by C-AFM on the surface of the graphene/polymer composite samples cut by microtome.^[12] However, some attempts to obtain 3-dimensional distribution of the sample properties measured by SPM were already done earlier.^[19–21] In the given work we present results of a 3-dimensional reconstruction of a single graphene cluster in the graphene/polystyrene composite by a new technique which is a combination of SPM and microtome.^[20,21]

2. Results and Discussion

2.1. Measurements with Different SPM Methods for Electrical Characterization

Figure 1 displays the general scheme of our experimental setup. The sample is fixed by the electrically grounded microtome holder and its surface is freshly cut by the microtome knife and subsequently investigated by SPM. In our following discussion the sample will be treated as a nonconductive matrix (PS) filled with conductive two-dimensional sheets of arbitrary shape, which are the graphene sheets. The surface of the sample is not completely flat after cutting and reveals vertical scratches and some inhomogeneities caused by the knife and the local sample properties (Figure 2a,b). The cross-section of the topography image shows height variations within 12 nm over the investigated 5 μm x 5 μm area (Figure 2b). Studying the graphene distribution inside the polymer matrix, e.g., by mechanical testing with SPM, using phase shift measurements in tapping mode, is difficult because of the small thickness of graphene sheets in the composite (one or few atomic layers). As a result a contact area between a tip and the graphene sheets is much smaller than the total tip-sample contact area (at least a few nanometers) and the contribution of the graphene properties to the measured signal is rather low. In addition, the surface inhomogeneities influencing phase image make image interpretation problematic (Figure 2a).

On the other hand, C-AFM allows for the easy distinguishing of nanoparticles of a conductive network inside the composite sample.^[21] We have measured the topography and

current distribution by C-AFM in contact mode with the tip-sample force of ~10 nN (Figure 2b, 2c). Such a force allows for nondestructive surface analysis: subsequent measurement in tapping mode on the same area does not reveal any changes of the sample surface. The current distribution image shows places where the conductive network of GS appears on the surface: all conductive areas in Figure 2c are electrically connected to the grounded back electrode through the volume of the composite sample (Figure 1a). GS appear at the surface with curved shapes, which corresponds to cross-sections of two-dimensional sheets with an arbitrary shape. The lateral resolution of C-AFM is limited by the tip-sample contact area, which can be estimated from Hertzian contact theory. The diameter of the contact between a spherical gold tip with the radius of 50 nm and PS surface is less than 10 nm at the tip-sample force of 10 nN. This result is in agreement with the measurements of full width at half maximum of the current signal for GS (Figure 2c). The graphene-based composites are convenient samples for estimation of the resolution of different SPM methods because of extremely small thickness of GS.

For the next step, phase-detecting EFM^[22–25] was utilized for measurements of the electrostatic interaction between a tip and a composite sample at the same area as for the case of C-AFM (Figure 2d). The interpretation of EFM images is not as straightforward as for C-AFM and needs more explanations, especially because of heterogeneous structure. The total electrostatic force acting on a biased cantilever during the second pass is (for any function $f(z)$ we imply: $f' \equiv \partial f / \partial z$, $f'' \equiv \partial^2 f / \partial z^2$)

$$F = F_{\text{cap}} + F_c \quad (1)$$

where $F_{\text{cap}} = C'(U_t - U_{\text{cp}})^2/2$ is the capacitive force, C is the tip-sample capacitance, U_t is the tip bias, U_{cp} is the tip-sample contact potential difference; F_c is the Coulomb force between surface charge q_s and tip charge q_t : $F_c = q_s q_t / (4\pi\epsilon_0 z^2)$, z is the tip-sample distance, ϵ_0 is the electric constant. Depending on tip position above the sample surface different forces will dominate. With phase-detecting EFM the measured signal is determined by the electrostatic force gradient.^[23,25] Taking into account the image charges, induced by the surface charges inside the tip, we have complete electrostatic force gradient in the form of:^[23,24]

$$F' = C'' \frac{(U_t - U_{\text{cp}})^2}{2} + \frac{q_s}{4\pi\epsilon_0 z^2} \left(\frac{2q_s}{z} + (U_t - U_{\text{cp}}) \left(C' - \frac{2C}{z} \right) \right) \quad (2)$$

If there are no surface charges ($q_s = 0$) the Equation 2 becomes:

$$F' = C''(U_t - U_{\text{cp}})^2/2 \quad (3)$$

Therefore, the phase shift above the graphene sheets in Figure 2d is determined by the second derivative of the tip-sample capacitance. The contrast of the PS matrix far away from the graphene sheets is influenced significantly by the gradient of the Coulomb force F_c between the biased tip and the surface charges. The phase contrast at GS is more pronounced

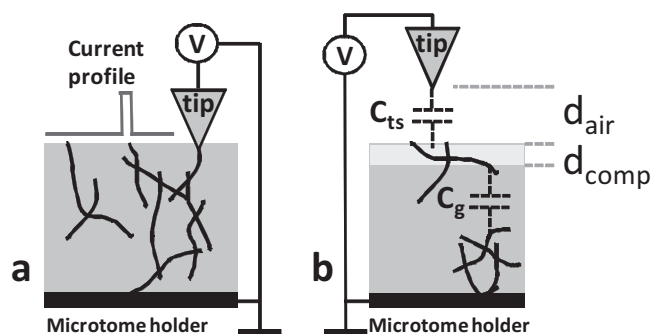


Figure 1. Scheme of experiment: a) C-AFM, b) EFM.

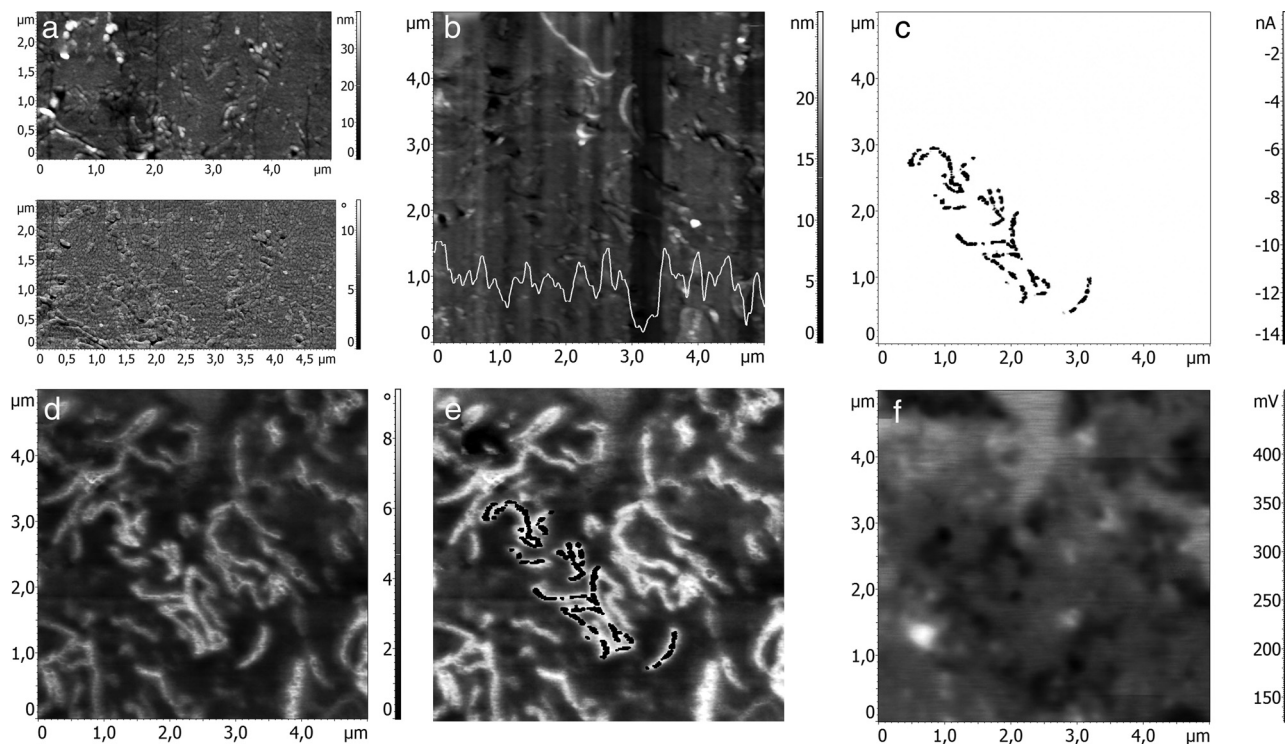


Figure 2. SPM images obtained on the surface of graphene/PS composite: a) topography (top) and phase image (bottom); b) topography and cross-section. The vertical scratches appear after microtome cutting. SPM results for area b): c) current distribution (C-AFM image) at $U_t = -1$ V; d) EFM phase image at $U_t = -2$ V; e) combined C-AFM and EFM images; f) surface potential (SKPM) image.

than that at the PS matrix, which can be explained by the influence of the high aspect ratio of GS resulting in the concentration of the electric field near the graphene edges. It is clearly visible in Figure 2d that more GS are revealed by EFM when compared with the corresponding current distribution image of the same area (Figure 2c). There are two main reasons for such phenomena. First of all, the electrostatic interaction can be observed by EFM also above GS, which are not electrically connected to the conductive network and thus behave as capacitors. Further, the long range character of electrostatic forces allows graphene sheets that are embedded into the matrix and don't appear at the surface to be also detected by EFM. Figure 2e shows a superposition of the EFM and C-AFM images acquired at the same sample area, which allows for straightforward distinguishing between GS connected to the conductive network and those unconnected or those covered by the matrix. In the following discussion terms “connected GS” and “unconnected GS” mean graphene sheets connected and unconnected to the conductive filler network, correspondingly.

We have performed scanning kelvin probe microscopy (SKPM) measurements to gain additional information on the local surface potential of the sample. Interestingly, the surface potential distribution measured by SKPM^[26,27] on the same area as previously investigated by C-AFM and EFM (Figure 2f) is completely different and does not reveal any clear structure related to the graphene network. The result of SKPM measurements at connected GS is approximately equal to U_{cp} . The SKPM contrast obtained at the PS matrix is determined mostly

by the surface charges q_s . With the point charge approximation the Coulomb force F_c at a frequency of cantilever mechanical resonance becomes equal to $F_c = \frac{q_s C U}{4\pi\epsilon_0 z^2}$, where U is the AC voltage applied to the tip.^[27] Then the SKPM signal above the nonconductive polymer matrix, which is the result of nullifying the tip-sample force (Equation 1), is $\frac{q_s C}{4\pi\epsilon_0 z^2 C_t} + U_{cp}$. Therefore, the absence of a clear signal from the GS network in Figure 2f is a result of insensitivity of SKPM to both capacitance and its derivatives above uncharged places. Poor SKPM contrast is also caused by its lower resolution when compared with the high resolution force gradient detection of EFM. The average level of surface potential in Figure 2f is around 0.3 V, which is approximately the gold tip-graphite contact potential difference. The contrast related to the deviation of surface potential from this level is related to the surface charges. The surface charges in PS also influence the EFM contrast (by F_c'), but they are less visible than the graphene edges. These charges appear either during composite film preparation or during cutting.

2.2. Peculiarities of EFM Imaging

The lateral resolution of EFM can be determined by measurements of full width at half maximum of the EFM phase signal at GS (Figure 2d). The smallest value measured at different GS is 30–40 nm, which is the EFM resolution in this case. The minimal electrostatic force gradient, which can be detected by EFM, is estimated by the formula $F'_{\min} = \sqrt{k k_B T \Delta f} / Q \pi f_1 / A_{\text{rms}}$,

where k is the cantilever force constant, k_B is the Boltzmann constant, T is the temperature, Δf is the measurement bandwidth, Q is the cantilever quality factor, f_1 is the cantilever resonant frequency, A_{rms} is the root-mean-square amplitude of cantilever.^[28] By using $\Delta f = 1$ kHz, $f_1 = 70$ kHz, $Q = 50$, $k = 0.6$ Nm⁻¹ and $A_{\text{rms}} = 10$ nm we get $F'_{\text{min}} \approx 5 \times 10^{-5}$ Nm⁻¹ at $T = 293$ K. In the case $F' \ll k$ the electrostatic force gradient measured above GS can be estimated by using $F' = k\Delta\phi/Q$ ^[29] where $\Delta\phi$ is the cantilever phase shift. For the phase shift of 11°, which is typical for GS in Figure 2d, we have $F' = 2 \times 10^{-3}$ Nm⁻¹, and then by using Equation 3: $C'' = 8 \times 10^{-3}$ Fm⁻² above GS at $U_t = -2$ V. We can estimate the value of surface charges q_s , which are present on the sample surface, by measurements of EFM phase image at $U_t = U_{\text{cp}}$. Then the contrast obtained by EFM is only the result of Coulomb interaction. In this case Equation 2 become: $F' = q_s^2/(2\pi\epsilon_0 z^3)$. The measured phase shift at $U_t = 0.3$ V is 3° and, using $F' = k\Delta\phi/Q$, we get a typical value of surface charge in the PS matrix in point charge approximation of $q_s = 3 \times 10^{-17}$ C.

One of the most important questions is: what is the distance d_{comp} (Figure 1b), at which EFM can detect the graphene edges inside the PS matrix? In order to answer this question the phase-distance curves were measured at $U_t = -2$ V above the graphene sheets (Figure 3). The data in Figure 3 were obtained by connected and unconnected GS, as well as the PS matrix. The similar behavior of phase-distance curves was observed above connected and unconnected GS but the amplitude of the signal was different (Figure 3). Such a difference is explained by an additional voltage drop inside the sample between GS when the signal above unconnected GS is measured. Then, corresponding to the Equation 3, the tip-unconnected GS voltage and, as consequence, the detected force gradient are reduced as well. The phase difference between connected GS, unconnected GS and matrix determines EFM contrast in Figure 2d. At a large tip-sample distance all three curves are overlapping, which is the result of a larger actual tip surface probing the signal; not only the tip end, but also the conical tip shape plays a role far above the surface.^[25] We have measured the

phase-distance curves above five different GS and at several different positions for all measured GS. The value of d_{air} for all measurements is 100–200 nm; maximal value 200 nm was obtained for one of the connected GS shown in Figure 3. Now we can roughly estimate the distance d_{comp} , at which graphene edges can be detected inside the PS matrix, by using the following equation:

$$d_{\text{comp}} \approx (d_{\text{air}} - d) / \epsilon_{\text{ps}} \quad (4)$$

where ϵ_{ps} is the relative permittivity of PS, d is the tip-sample distance during EFM measurements. Parameter d in Equation 4 takes into account the fact that EFM measurement is performed at certain tip-sample distance, which reduces d_{comp} . Using $\epsilon_{\text{ps}} = 2.5$, the range $d_{\text{air}} = 100$ –200 nm and $d = 25$ nm, for the conditions applied in our EFM measurements we can estimate $d_{\text{comp}} \sim 30$ –70 nm, which means that EFM images consist of information from a top thin layer of the composite sample rather than pure surface contrast. The value of d_{air} is similar for different tips, which means sensitivity of EFM to the structures under the composite surface is determined mostly by the relative permittivity of the polymer matrix.

In order to explain qualitatively the phase difference between connected and unconnected GS in terms of capacitance, let us discuss a simple model for a single GS laying at the composite surface. Total capacitance C in Equation 3 can be divided into two parts: $1/C(z) = 1/C_{\text{ts}}(z) + 1/C_s$, where $C_{\text{ts}}(z)$ is the capacitance between tip and GS, calculated for the distance d_{comp} inside the sample, and C_s is the capacitance between GS for the remaining sample volume (Figure 1b). Here C_s is constant and $C_{\text{ts}}(z)$ depends on the tip-sample distance z . Then the second derivative of C is:

$$C'' = \frac{C_s^2}{(C_{\text{ts}} + C_s)^2} \left(C_{\text{ts}}'' - \frac{2C_{\text{ts}}'^2}{(C_{\text{ts}} + C_s)} \right) \quad (5)$$

In the case of connected GS, we can expect a very large capacitance C_s of the sample in comparison with the tip-sample capacitance C_{ts} due to the large total surface of the graphene sheets and a large distance between electrodes. In this case $C_s \gg C_{\text{ts}}$ and Equation 5 becomes

$$C'' \approx C_{\text{ts}}'' - 2C_{\text{ts}}'^2 / C_s \quad (6)$$

It is easy to check that for a flat condenser $C'' \approx C_{\text{ts}}''$; this approximation will be valid also when the gradient of C_{ts} in Equation 6 is small enough. It is not possible to obtain an analytical expression for the capacitance C_{ts} between tip and GS because of the complicated and unknown geometry. Probably the best approach to tackle this problem is to approximate the capacitance between two planes inclined under different angles. Such a problem can be solved by using a conformal transformation^[30,31] and the result can be written in terms of Bessel functions and elliptical integrals. The numerical simulation for two perpendicular planes^[31] reveals smaller dependence of the capacitance on tip-sample distance in comparison with the case of the parallel flat condensers. Based on this fact, we can expect that $C'' \approx C_{\text{ts}}''$ for most of connected GS. For unconnected GS separated from the conductive network through one gap placed below d_{comp} : $C_s \approx C_{\text{gap}}$ in Equation 5, where C_{gap} is the capacitance of the gap. Finally, in terms of capacitance, the

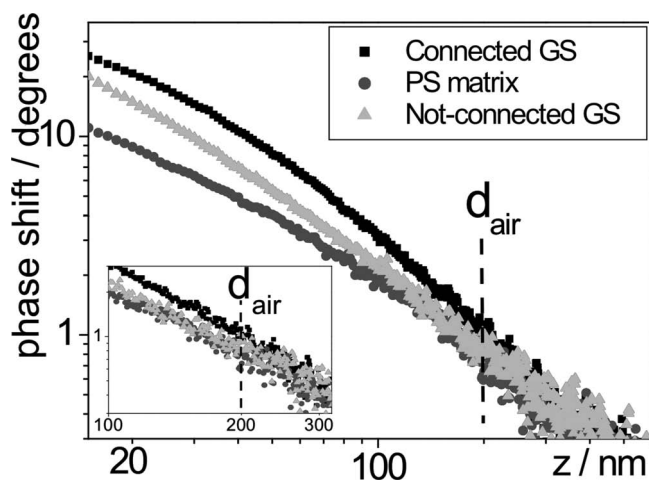


Figure 3. Phase-distance dependences for connected GS, unconnected GS and PS matrix. The cantilever free amplitude is 15 nm.

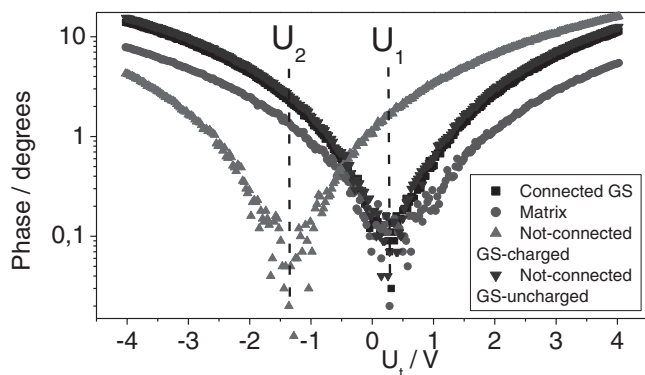


Figure 4. Log (phase)-tip voltage dependences for different graphene sheets and PS. Here the curves for the connected GS and the unconnected uncharged GS are close to each other.

phase difference between connected GS and unconnected GS is explained by different C'' in Equation 3, as calculated by Equation 5.

Another reason for such a phase difference should be discussed as well: namely, charging of unconnected GS, which are electrically isolated. Corresponding to Equation 2, at fixed tip-sample distance the phase-voltage dependence has the form of a parabola. Above conductive surfaces the minimum of the parabola corresponds to the tip-sample contact potential difference. If charges are involved then the minimum of the parabola will be shifted due to the Coulomb interaction.^[24] In **Figure 4** several phase-voltage plots are shown for different positions on the sample surface. The logarithmic scale for the phase was used in order to determine the position of the parabola minimum more precisely. Most of the measured phase-voltage curves above connected GS, unconnected GS and the PS matrix have their minimum at $U_1 = 0.3$ V, which is approximately the gold tip-graphite contact potential. Small deviations of the minimum from U_1 for PS can be explained by the influence of surface charges; we have demonstrated their

presence in **Figure 2f**. However, on some of the unconnected GS, the minimum of parabola is shifted up to few volts from U_1 . In **Figure 4** the parabola minimum of one of unconnected GS curves is located at $U_2 = -1.3$ V, which is the result of the charge influence. Charged unconnected GS have been observed just after cutting, which means that the sample preparation route involving mechanically cutting the fresh sample surface by the microtome diamond knife can induce charges. Also charging and discharging of some of unconnected GS were often observed during measurements, which are explained by the influence of the biased tip. Recharging processes can be visualized by both SKPM and EFM measurements, but such processes are beyond experimental control. On the contrary, recharging phenomena were never observed at the location of connected GS; all measured connected GS have their minimum of the phase-voltage curve at U_1 .

Figure 5 shows two EFM images subsequently acquired at the same area for $U_t = -2$ V and -6 V. Looking to Equation 2 we can expect that the contrast difference between images acquired at different voltages is a result of a better signal to noise ratio caused either by the C dependency on U_t or the increased U_t , which leads to a larger d_{comp} . Observation of almost identical features in **Figures 5a** and **5b** are explained by the small additional amount of GS edges detected in **Figure 5b**. The little change of contrast is mainly located at areas surrounding GS: the features appear wider at higher voltage because of a larger d_{comp} . In other words, EFM has worse resolution at higher voltages due to larger volume of tip-sample interaction. These statements are confirmed by our results in **Figure 5**, where details related to the internal GS network structure are better visible at lower voltage. In our measurements we found that $U_t = -2$ V gives an optimal ratio of sensitivity and resolution for the graphene/PS composite under investigation. Analysis of the phase difference between PS matrix and the GS reveals saturation of contrast: the EFM phase contrast for -4 V and -6 V is approximately the same (**Figure 5d**). Similar saturation and even reduction of EFM phase contrast at high tip-sample potential difference has been observed earlier for carbon nanotubes/

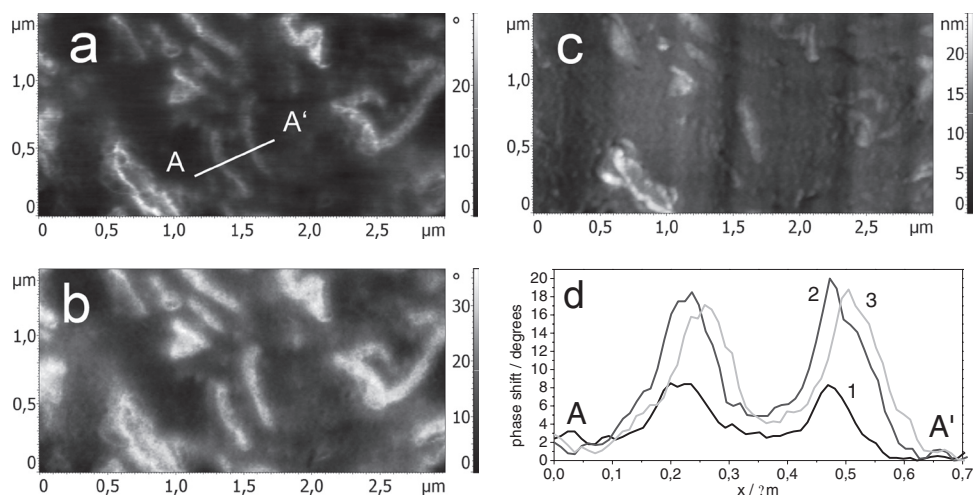


Figure 5. EFM images of the same area at: a) $U_t = -2$ V, b) $U_t = -6$ V; c) topography of measured area; d) cross-section AA' at $U_t = -2$ V (1), $U_t = -4$ V (2), $U_t = -6$ V (3).

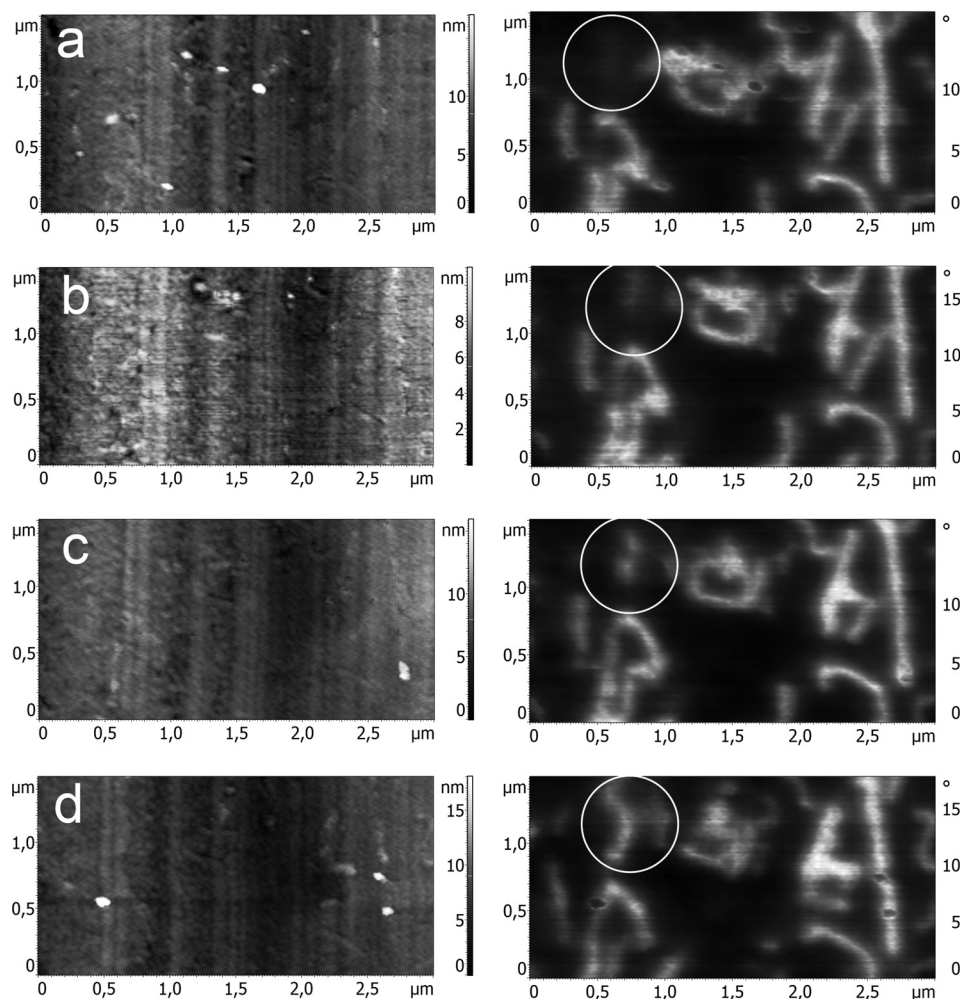


Figure 6. Appearance of the graphene edge (inside circle). Topography (left column) and corresponding EFM images (right column) obtained on the same area with the microtome step $\Delta s = 30$ nm: a) $z = 0$ nm, b) $z = 30$ nm, c) $z = 60$ nm, d) $z = 90$ nm.

polymer composite;^[32] such behavior can be related to polarization processes. Saturation has also been obtained for d_{air} from analysis of the phase–distance curves at different U_t for the same connected GS shown in Figure 3: d_{air} reaches its maximal value at $U_t \sim -3$ V. Value of d_{air} for voltages from -3 V to -6 V is up to 300 nm, which means maximal $d_{\text{comp}} \sim 110$ nm for the tip-sample voltage range $0 \div 6$ V, using $d = 25$ nm in Equation 4.

The value of d_{comp} can also be estimated by another experiment using a combination of SPM and microtome. For this purpose sequential cutting of the sample surface was performed by applying the microtome. A series of EFM images at $U_t = -3$ V was obtained from the same area, each image was obtained after removing a layer with a thickness of $\Delta s = 30$ nm (Figure 6). From Figure 6 we can see that we need three cuts or removal of a 90 nm layer before graphene edges appear with maximal contrast and now are located at the free surface of the sample, which means $d_{\text{comp}} \sim 60$ –90 nm. The GS shown in Figure 6 is connected to the conductive network and then d_{comp} is close to its maximal value. By taking into account $d = 25$ nm used in the measurements, the maximal possible depth of sensing should be increased $d_{\text{comp}} \sim 70$ –100 nm. This range is close to the value

of $d_{\text{comp}} \sim 110$ nm obtained from the d_{air} measurements. The estimation of d_{comp} based on removing slices from the sample surface is more reliable, because Equation (4) is empirical and based mainly on an analysis of our experimental results, which make it suitable only for a very rough estimation of d_{comp} . The more precise evaluation of d_{comp} from phase-distance measurements needs a detailed analysis of the second derivative of the tip-GS capacitance, which, in some approximation, can be described by Equation 5.

2.3. 3D Reconstruction of Morphology

By using such a technique utilizing consequent microtome cutting and SPM measurements, it is possible to reconstruct the distribution of electrical properties inside the sample with nanometer resolution. The method of 3D reconstruction of properties measured by SPM was described recently.^[20] Later, 3D reconstruction of conductive network in carbon nanotubes/PS composite was performed with the help of C-AFM.^[21] Here we apply such a method for 3D reconstruction of a single

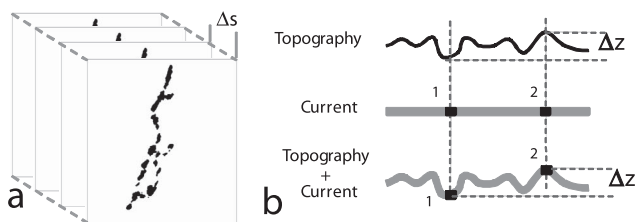


Figure 7. Scheme of 3D conductivity distribution reconstruction: a) 3D image formation, b) principle of C-AFM data correction with topography taken into account. The spots 1 and 2 represent conductive places.

graphene cluster in graphene/PS composite. A series of 28 current distribution images were obtained with a microtome step of 12 nm. 3D current distribution is reconstructed by alignment of conventional 2D scans separated by a distance of 12 nm, which resulted in the reconstructed volume of $2.5 \mu\text{m} \times 2.5 \mu\text{m} \times 0.34 \mu\text{m}$. C-AFM images (Figure 2c) consist of information about distribution of conductive places in the xy plane. However, in reality, conductive areas are also placed at different z coordinates, corresponding to the height image measured at the same time (Figure 2b). The standard procedure of 3D current distribution image formation implies alignment of two-dimensional current images at constant distance, which is equal to the microtome slice thickness Δs (Figure 7a). Such situation is acceptable when thickness of microtome slice Δs is much larger than height variations Δz . In our case slice thickness Δs and typical peak-to-valley roughness of height image are 12 nm and 10–15 nm, respectively. This means that redistribution of measured conductive areas along the z -axis in accordance with height image is necessary. A principle of the new correction procedure for the obtained data by using topography information is described in Figure 7b. This procedure should be used when surface roughness caused by knife imperfections, moving particles or sample properties is comparable with the value of the microtome step. The 3D reconstruction of the graphene cluster after application of the correction procedure is shown in Figure 8. By using C-AFM we can only reconstruct the network of connected GS. It is possible to perform reconstruction of network, consisting of both unconnected GS and connected GS, based on EFM images (Figure 6), but then the z -resolution will be reduced because of the long-range character of the electrostatic interaction. The large horizontal size of the conductive spots visible in cross-sections (Figure 8b) is explained by convolution with the tip, as well as sectioning at some angle in respect to the GS plane. The connection of two

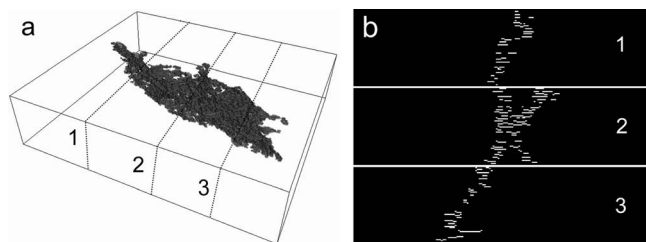


Figure 8. a) 3D reconstruction of the graphene cluster; b) the xz cross-sections of a). The reconstructed volume is $2.5 \mu\text{m} \times 2.5 \mu\text{m} \times 0.34 \mu\text{m}$ (the z scale differs from the xy scale for the reason of better visibility).

graphene sheets is visible in cross-section in the middle part of cluster (Figure 8b). GS in Figure 8 are predominantly aligned along the film plane, which is the result of compressing. Such a technique of volume properties reconstruction enables the control of the shape of individual GS in graphene-based composites. After application of the described correction procedure, the accuracy of the slice thickness Δs is the main possible source of 3D image distortion. Accuracy of microtome sample holder movement is within 0.5% from the preset value. However, the real slice thickness depends on many different factors: sample mechanical properties, cutting settings etc. We have deposited several slices cut by microtome on the mica, and then the thickness of the deposited slices has been checked by AFM. The deviation of measured thickness from the preset value was within 20%.

3. Conclusions

GS connected and unconnected to the conductive network in graphene-based conductive composites can be clearly distinguished by measuring the same sample area with C-AFM and EFM. The different EFM signal obtained at the location of connected GS and unconnected GS is explained by additional voltage drop between unconnected GS, charging of some unconnected GS and, in some cases, by detecting GS below the surface. EFM is able to detect structure under the surface, e. g. the contrast obtained at $U_t = -3$ V and tip-sample distance of 25 nm consists of information about the GS distribution down to ~ 60 – 90 nm from the surface. The resolution of EFM images is decreased when higher voltages are used, because of the larger volume of tip-sample interaction. 3D reconstruction of the individual GS in the polymer matrix with a newly developed correction procedure allows for a more precise volume reconstruction of properties and study of local organization of the graphene network on the nanoscale. The introduced approach can be applied for other polymer composites filled with conductive nanoparticles.

4. Experimental Section

Graphene/PS Composite: The composite studied by us was prepared by the latex technology,^[12,33–35] which enables incorporation of nanofillers into any kind of highly viscous polymer synthesized by emulsion polymerization. Materials used were PS latex, which was synthesized from aqueous styrene/sodium dodecyl sulfate emulsion (28.16 wt% solids), and SP-2 Graphite from Bay Carbon that was used as a filler. Graphene was synthesized via oxidation of graphite (Hummers method^[36]) and subsequent reduction in the presence of polystyrenesulfonate (PSS), following the method described by Stankovich et al.^[6] After the synthesis graphene covered with PSS was filtered and dried under vacuum. The product was then mixed with aqueous PS latex, the mixture was frozen in liquid nitrogen for several minutes and water was removed with a Christ Alpha 2–4 freeze dryer operated at 0.2 mbar and 20 °C overnight. The resulting composite powder was compressed into films at 180 °C between Teflon sheets with a Collin Press 300G. More details about sample preparation can be found in reference.^[12] In the present work we have studied in detail a composite with 1.9 wt% of graphene. Such a concentration is above percolation threshold, which is around 1.0 wt%.^[12]

SPM Measurements: The SPM Ntegra Tomo (NT-MDT Co.) designed for 3D property reconstruction has been used. This device is a combination of a microtome (Leica) with a scanning probe microscope

in “scanning by tip” configuration.^[20,21] With this setup the sample is fixed by the conventional microtome sample holder and after cutting by oscillating diamond knife (Diatome) the fresh sample surface is analyzed by SPM. C-AFM measurements were performed in contact mode with voltage $U_t = -1$ V applied to the tip (Figure 1a). EFM and SKPM measurements were executed in two passes, performed line by line. During the first pass topography is measured and stored by the software. During the second pass the scanner moves the cantilever above the same line, corresponding to the stored profile, at a certain tip sample separation, which is pre-set in the software. With phase-detecting EFM the oscillating cantilever phase shift is detected during the second pass, which is determined by long-range electrostatic interaction.^[22–25] At the second pass the probe is biased, and the sample is grounded through the microtome holder (Figure 1b). Furthermore, during the second pass of SKPM the cantilever oscillations, induced by AC voltage between tip and sample at cantilever mechanical resonance frequency, are nullified by DC voltage applied to the tip at each point of the scan. This DC voltage is equal to the tip-sample contact potential difference.^[26,27] Conductive cantilevers NSC36, lever C (Micromash) covered by Cr and Au layers were used in our experiments. The tips have approximately conical shape and average tip radius is around 50 nm. The composite sample is a film with thickness of approximately 50 μm , which was incorporated into epoxy resin for mechanical stability during cutting and which was electrically connected with the microtome sample holder. Topography measurements were performed with the free cantilever amplitude $A_0 = 50\text{--}70$ nm and the set-point amplitude $\sim 0.5 A_0$. During EFM imaging (second pass) $A_0 = 15$ nm; the tip-sample distance during second pass was $d = 25$ nm for both EFM and SKPM.

All phase-distance measurements were performed point by point along a predefined line for a more accurate determination of the position above the object of interest. Each phase-distance curve is the average of 3 independent measurements. In Figure 3, $z = 0$ corresponds to the surface; phase shift is 0 at $z = 700$ nm for all curves. Free amplitude of cantilever oscillations used for results shown in Figure 3 and Figure 4 was 15 nm. The scanned sample surface is perpendicular to the film plane. The sample length (the distance between SPM tip and grounded electrode) is about 5 mm.

3D Reconstruction by SPM: Algorithm of 3D reconstruction implies alternate microtome cutting and measurements of the same area by SPM. As a result of this procedure a stack of SPM images is obtained having a Δs (thickness of each section) down to 10 nm. This array of scans can be aligned in one 3D image by a simple procedure, which is used, for example, in the so-called “slice and view” technique applying a focused ion beam machine for slicing and a scanning electron microscope viewing. It is possible to use different SPM methods in order to reconstruct three-dimensional distribution of electrical, mechanical, magnetic and other properties at the nanoscale.^[20,21] Commercial software AMIRA and script written for MATLAB were used for 3D image processing.

Acknowledgements

The authors thank Dr. A. Efimov (Institute for Transplantology and Artificial Organs, Russia), A. Volkov (University of Erlangen, Germany) Dr. R. Ranner (Leica Microsystems, Austria), Prof. Dr. C. Koning and Dr. G. G. Hoffmann (Eindhoven University of Technology, The Netherlands) for helpful discussions. This work was supported by Dutch Polymer Institute (projects #615 and #648). A. A., Yu. S., O. A., and J. L. acknowledge the Federal Program “Scientific and educational research personnel of innovative Russia” 2009-2013 (the contract 02.740.11.5119).

Received: August 3, 2011

Revised: October 15, 2011

Published online: February 10, 2012

- [1] A. K. Geim, K. S. Novoselov, *Nat. Mater.* **2007**, *6*, 183.
- [2] M. Katsnelson, *Mater. Today* **2007**, *10*, 20.
- [3] C. Soldano, A. Mahmood, E. Dujardin, *Carbon* **2010**, *48*, 2127.
- [4] D. R. Dreyer, S. Park, C. W. Bielawski, R. S. Ruoff, *Chem. Soc. Rev.* **2010**, *39*, 228.
- [5] S. H. Lee, D. R. Dreyer, J. An, A. Velamakanni, R. D. Piner, S. Park, Y. Zhu, S. O. Kim, C. W. Bielawski, R. S. Ruoff, *Macromol. Rapid Commun.* **2010**, *31*, 281.
- [6] S. Stankovich, D. A. Dikin, G. H. B. Dommett, K. M. Kohlhaas, E. J. Zimney, E. A. Stach, R. D. Piner, S. T. Nguyen, R. S. Ruoff, *Nature* **2006**, *442*, 282.
- [7] T. Ramanathan, A. A. Abdala, S. Stankovich, D. A. Dikin, M. Herrera-Alonso, R. D. Piner, D. H. Adamson, H. C. Schniepp, X. Chen, R. S. Ruoff, S. T. Nguyen, I. A. Aksay, R. K. Prud'Homme, L. C. Brinson, *Nat. Nanotechnol.* **2008**, *3*, 327.
- [8] S. Ansari, E. P. Giannelis, *J. Polym. Sci. B* **2009**, *47*, 888.
- [9] H. Kim, C. W. Macosko, *Macromolecules* **2008**, *41*, 3317.
- [10] H. Zhang, W. Zheng, Q. Yan, Y. Yang, J. Wang, Z. Lu, G. Ji, Z. Yu, *Polymer* **2010**, *51*, 1191.
- [11] H. Pang, T. Chen, G. Zhang, B. Zeng, Z. Li, *Mater. Lett.* **2010**, *64*, 2226.
- [12] E. E. Tkalya, M. G. Ghislandi, A. Alekseev, J. Loos, C. E. Koning, *J. Mater. Chem.* **2010**, *20*, 3035.
- [13] D. Cai, M. Song, *J. Mater. Chem.* **2010**, *20*, 7906.
- [14] R. Verdejo, M. M. Bernal, L. J. Romasanta, M. A. Lopez-Manchado, *J. Mater. Chem.* **2011**, *21*, 3301.
- [15] T. Kuilla, S. Bhadra, D. Yao, N. H. Kim, S. Bose, J. H. Leea, *Prog. Polym. Sci.* **2010**, *35*, 1350.
- [16] J. R. Potts, D. R. Dreyer, C. W. Bielawski, R. S. Ruoff, *Polymer* **2011**, *52*, 5.
- [17] R. Strumpler, J. Glatz-Reichenbach, *J. Electroceram.* **1999**, *3*, 329.
- [18] A. V. Kyrlyuk, P. van der Schoot, *Proc. Natl. Acad. Sci. USA* **2008**, *105*, 8221.
- [19] R. Magerle, *Phys. Rev. Lett.* **2000**, *85*, 2749.
- [20] A. E. Efimov, A. G. Tonevitsky, M. Dittrich, N. B. Matsko, *J. Microsc.* **2007**, *226*, 207.
- [21] A. Alekseev, A. Efimov, K. Lu, J. Loos, *Adv. Mater.* **2009**, *21*, 4915.
- [22] Y. Martin, D. W. Abraham, H. K. Wickramasinghe, *Appl. Phys. Lett.* **1988**, *52*, 1103.
- [23] B. D. Terris, J. E. Stern, D. Rugar, H. J. Mamin, *Phys. Rev. Lett.* **1989**, *63*, 2669.
- [24] H. Bluhm, A. Wadas, R. Wiesendanger, *Phys. Rev. B* **1997**, *55*, 4.
- [25] J. Kim, J. P. Hinstroza, W. Jasper, R. L. Barker, *Fibers Polym.* **2011**, *12*, 89.
- [26] M. Nonnenmacher, M. P. O'Boyle, H. K. Wickramasinghe, *Appl. Phys. Lett.* **1991**, *58*, 2921.
- [27] P. Girard, *Nanotechnology* **2001**, *12*, 485.
- [28] T. R. Albrecht, P. Grütter, D. Horne, D. Rugar, *J. Appl. Phys.* **1991**, *69*, 668.
- [29] S. N. Magonov, V. Elings, M.-H. Whangbo, *Surf. Sci.* **1997**, *375*, L385.
- [30] B. N. Das, S. Ananda Mohan, K. V. S. V. R. Prasad, *IEEE Trans. Electromagn. Compatibil.* **1985**, *EMC-27*, 96.
- [31] Y. Xiang, *J. Electrostat.* **2008**, *66*, 366.
- [32] M. Zhao, X. Gu, S. E. Lowther, C. Park, Y. C. Jean, T. Nguyen, *Nanotechnology* **2010**, *21*, 225702.
- [33] O. Regev, P. N. B. ElKati, J. Loos, C. E. Koning, *Adv. Mater.* **2004**, *16*, 248.
- [34] N. Grossiord, J. Loos, C. E. Koning, *J. Mater. Chem.* **2005**, *15*, 2349.
- [35] N. Grossiord, J. Loos, O. Regev, C. E. Koning, *Chem. Mater.* **2006**, *18*, 1089.
- [36] W. S. Hummers, R. E. Offeman, *J. Am. Chem. Soc.* **1958**, *80*, 1339.